

Efficient Piecewise Training of Deep Structured Models for Semantic Segmentation

Guosheng Lin, Chunhua Shen, Ian Reid, Anton van den Hengel

The University of Adelaide, Australia; and Australian Centre for Robotic Vision

Abstract—Recent advances in semantic image segmentation have mostly been achieved by training deep convolutional neural networks (CNNs) for the task. We show how to improve semantic segmentation through the use of contextual information, by combining the strengths of deep CNNs to learn powerful feature representations, with Conditional Random Fields (CRFs) which can capture contextual relation modeling. Unlike previous work, our formulation of “deep CRFs” learns both unary *and* pairwise terms using multi-scale fully convolutional neural networks (FCNNs) in an end-to-end fashion, which enables us to model complex spatial relations between image regions. A naive method for training such an approach would rely on direct likelihood maximization of the CRF, but this would require expensive inference at each stochastic gradient decent iteration, rendering the approach computationally unviable. We propose a novel method for efficient joint training of the deep structured model based on piecewise training. This approximate training method avoids repeated inference, and so is computationally tractable. We also demonstrate that it yields results that are competitive with the state-of-art in semantic segmentation for the PASCAL VOC 2012 dataset. In particular, we achieve an intersection-over-union score of 70.7 on its test set, which outperforms state-of-the-art results that make use of the same size training set, thus demonstrating the value of our deep, multi-scale approach to modelling contextual relations.

CONTENTS

I	Introduction	1
II	Related work	2
III	Overview of our method	2
III-A	Potential networks	3
IV	Deep convolutional CRFs	3
IV-A	CRF training	5
IV-B	Piecewise training of CRFs	5
V	Experiments	6
V-A	Implementation details	6
V-B	Evaluation of different settings	6
V-C	Detailed evaluation of potentials	7
V-D	Comparison on the test set	7
V-E	Discussion	8
VI	Conclusions	8
	Appendix	8
	References	13

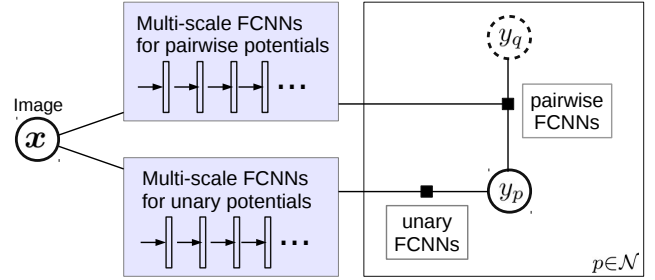


Fig. 1 – An illustration of our general CRF graph. Both our unary and pairwise potentials are formulated as multi-scale FCNNs which are learned in an end-to-end fashion.

I. INTRODUCTION

Semantic image segmentation aims to predict a category label for every image pixel, which is an important yet challenging task for image understanding. Recent approaches have applied convolutional neural network (CNNs) [11], [26], [2] to this pixel-level labeling task and achieved remarkable success. Among these CNN-based methods, fully convolutional neural networks (FCNNs) [26], [2] have become a popular choice, because of their computational efficiency for dense prediction and end-to-end style learning.

Contextual information provides important cues for scene understanding tasks. Spatial context relations can be formulated in terms of semantic compatibility relations between one object and its neighboring objects or image patches (stuff), in which a compatibility relation is an indication of the co-occurrence of visual patterns. For example, a car is likely to appear over a road, and a glass is likely to appear over a table. Context can also encode incompatibility relations. For example, a car is not likely to be surrounded by sky. Contextual relationships are ubiquitous. These relations also exist at finer scales, for example, in object part-to-part relations, and part-to-object relations. In some cases, contextual information is the most important cue, particularly when a single object shows significant visual ambiguities. A more detailed discussion of the value of spatial context can be found in [17].

Recent CNN-based segmentation methods often do not *explicitly* model contextual relations. In our work we propose to explicitly model the contextual relations using conditional random fields (CRFs). We jointly train FCNNs and CRFs to combine the strength of CNNs in forming powerful feature representations and CRFs in complex relation modeling. Some recent (unpublished) methods exist which combine CNNs and CRFs for semantic segmentation, e.g., the work in [2], [31].

However, these methods only consider the Potts-model-based pairwise potentials for enforcing smoothness. Although their unary potentials are based on CNNs, their pairwise potentials are still conventional log-linear functions. In contrast, we learn more general pairwise potentials also using CNNs to model the semantic compatibility between image regions. Overall, we formulate both the unary and pairwise potentials as multi-scale FCNNs for learning rich background context and modeling complex spatial relations, which is illustrated in Fig. 1.

Incorporating general pairwise potentials usually involves expensive inference, which brings challenges for CRF learning. To facilitate efficient joint learning of FCNNs and CRFs, we propose to apply piecewise training [33] to avoid repeated inference.

Thus our main contributions are as follows.

- We take advantage of the strength of CNNs in learning representations and CRFs in relation modeling. As in conventional CNNs, the training of our model is performed in an end-to-end fashion using back-propagation, but to make learning tractable, we propose to perform approximate training, using piecewise training of CRFs [33]. This avoids the repeated inference that would be necessary at every gradient descent iteration, which would be computationally unviable since hundreds of thousands or even millions of iterations are required for deep model training.
- We formulate CNN based general pairwise potential functions to explicitly model complex spatial relations between image patches. We consider multiple types of pairwise potential functions for modeling various spatial relations, such as “surrounding” and “above/below”.
- Multi-scale features have advantages in encoding background contextual information. We model both unary and pairwise potential functions by multi-scale FCNNs. We develop a network architecture to accept multi-scale image inputs with arbitrary sizes.
- Our model is trained on the VOC dataset alone (with augmented annotations) with no extra data; and we achieve a competitive intersection-over-union score of 70.7 on its test set, that outperforms the published state-of-the-art using the same training dataset.

II. RELATED WORK

Exploiting contextual information has been widely studied in the literature, e.g., the work in [30], [17], [5], [6]. For example, the early work “TAS” [17] models different types of spatial context between *Things* and *Stuff* using a generative probabilistic graphical model.

However the most successful recent method are based on CNNs. A number of these existing CNN-based methods for segmentation are region proposal based methods [13], [15], which first generate region proposals and then assign category labels to each region. Very recently, FCNNs [26], [2], [4] have become a popular choice for semantic segmentation, because of their effective feature generation and end-to-end training. FCNNs have also been applied to a range of other dense-prediction tasks recently, such as image restoration [8],

image super-resolution [7] and depth estimation [9], [24]. The method we propose here is similarly built upon fully convolution-style networks.

Combining the strengths of CNNs and CRFs for segmentation has been the focus of several recently developed approaches. DeepLab-CRF in [2] trains FCNNs and applies a dense CRF [21] method as a *post-processing* step. The method in [31] extends DeepLab and [22] by jointly learning the dense CRFs and CNNs. However, they only consider a special form of pairwise potential functions which enforce smoothness. Moreover, their pairwise potential functions are not CNNs. They require marginal computation in the training procedure. Unlike either of these methods, our approach jointly trains CNNs and CRFs, learning CNN-based general pairwise potential functions.

Jointly learning CNNs and CRFs has also been explored in other applications apart from segmentation. The recent work in [24], [25] proposes to jointly learn *continuous* CRFs and CNNs for depth estimation from a single image. They focus on continuous value prediction, while our method is for categorical label prediction. The work in [34] combines CRFs and CNNs for human pose estimation. During fine-tuning they simply drop the partition function for a loose approximation. The concurrent work in [3] explores joint training of Markov random fields and deep neural networks for the tasks of predicting words from noisy images and image multi-class classification. They assume that the energy function can be formulated as a sum of local functions. They need to compute the marginals for every gradient calculation, which can be very computationally expensive. For a segmentation task which involves a large number of nodes and edges, this approach might become impractically slow.

Recent segmentation methods in [26] (FCN) and [27] have demonstrated the performance of multi-scale CNN features. FCN generates multi-scale features from the middle layers of CNNs, while our method generates multi-scale features from multi-scale image inputs.

III. OVERVIEW OF OUR METHOD

An overview of our method is given in Figs. 2 and 4 with multiple deep networks providing both unary and pairwise terms to a CRF. The connectivity of the CRF is based on different spatial relations, and each type of spatial relation is modeled by a specific network for the pairwise potentials. The motivation for this is to allow neighboring nodes to provide contextual information to aid predictive power.

Within the present work we consider the two types illustrated in Fig. 3: “surrounding” and “above/below”. A CRF node is connected to all other nodes which lie within a range box. It would be straightforward to construct further pairwise potentials, either by varying the sizes or positions of the connection range boxes, and of course our approach is not limited to connections within “boxes”.

We construct asymmetric potential functions to model asymmetric spatial relations, e.g., “above/below”. More details are described in Section IV. With our general formulation of pairwise potentials, asymmetric properties can be easily

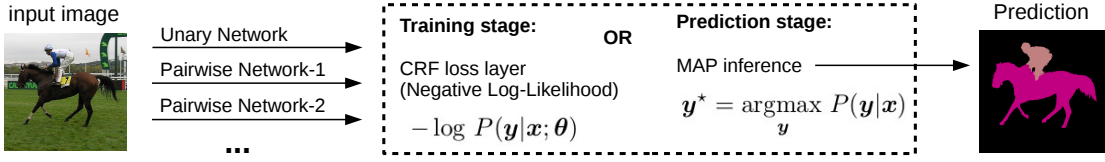


Fig. 2 – An illustration of the training and prediction process for one input image. An input image is fed into one unary and M pairwise potential networks. During the training, all network outputs go through a CRF loss layer. When performing prediction, a segmentation prediction is produced by solving the CRF MAP inference. Details of an unary or pairwise potential network are shown in Fig. 4.

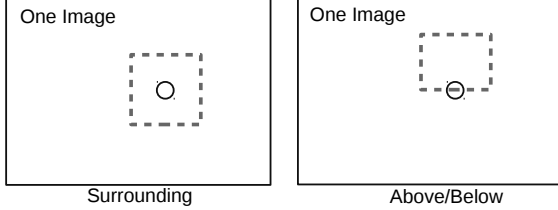


Fig. 3 – An illustration of two types of spatial relations, which corresponds to two types of pairwise potential functions. A node is connected to all other nodes which lie within the dash box.

achieved. Asymmetric potentials have also been studied in [35], [16] for modeling object layouts.

Our method explores different types of context. In the PASCAL VOC dataset [10], the image regions of 20 object categories are labeled in the training data, and all remaining regions are labeled as “background”. As discussed in [12], [17], the objects and “background” respectively correspond to the notion of “things” and “stuff”. Our pairwise connections cover the relations between object and background patches. Hence our pairwise potentials learn the *Thing-Thing*, *Stuff-Thing* and *Stuff-Stuff* context [17]. Another type of context is *Scene-Thing* context [17] which considers the scene-level information. Our multi-scale FCNNs generate features from large background regions, thus we implicitly learn the *Scene-Thing* context. Both our unary and pairwise potentials are constructed by multi-scale FCNNs, thus the *Scene-Thing* context are captured in all potentials.

A. Potential networks

Fig. 2 illustrates the training and prediction processes for one input image. We define one type of unary potential and M types of pairwise potentials, and construct one network for each potential function. Unlike conventional CRFs with log-linear potentials, both our unary and pairwise potential functions are modeled by multi-scale FCNNs. Learning FCNN base potentials enables powerful pairwise feature learning together with potential function learning in an end-to-end learning fashion, avoiding conventional hand designed pairwise features. Moreover, FCNNs are nonlinear functions and thus have much better fitting capacity than the linear function, which is beneficial for discovering patterns from complex pairwise relations.

Our potential networks have the same architecture, but do not share network parameters. During training, all potential network outputs pass through to a (common) CRF loss layer. At test time, prediction is performed by solving the CRF MAP

inference, which produces a pixel-wise labelled segmentation of the image.

Fig. 4 shows the details of one unary/pairwise potential network, which is a multi-scale FCNN. The importance of using multi-scale features to capture rich background contextual information is demonstrated in our experiments. On the left side of the figure an input image is resized into 3 scales, then each rescaled image goes through 6 convolution blocks (“Network Part-1”) to output 3 feature maps. The detailed configuration of potential networks is described in Fig. 5, and is based on the VGG-16 model [32]. The resulting 3 feature maps are of different sizes, but we then upscale the two smaller ones to the size of the largest feature map using nearest-neighbor interpolation, as also used in [25]. These feature maps are then concatenated to form one feature map.

The CRF graph is constructed based on the size of the largest output feature map, so that one node in the CRF graph corresponds to one spatial position of the feature map. We construct features for CRF nodes or edges from the concatenated feature map. The (multiple scale) features for one node or edge are passed through 2 fully connected layers (“Network Part-2”) to generate the potential output.

For the unary potential, the features for one CRF node is simply the corresponding feature vector in the feature map. The last layer of “Network Part-2” has K output units, where K is the number of classes to be considered.

The pairwise potentials are analogous except that – following the work in [19] – we concatenate the corresponding features of two connected nodes to obtain the CRF edge features. The last layer of “Network Part-2” has K^2 output units to match the number of possible label combinations for a pair of nodes. The ordering of the concatenation results in an asymmetric potential.

IV. DEEP CONVOLUTIONAL CRFS

We now describe the details of the CRF learning and prediction. We denote by $\mathbf{x} \in \mathcal{X}$ one input image and $\mathbf{y} \in \mathcal{Y}$ the labeling mask. The energy function is denoted by $E(\mathbf{y}, \mathbf{x}; \theta)$ which models the compatibility of the input-output pair, with a small output value indicating high confidence in the prediction \mathbf{y} . All network parameters are denoted by θ which we need to learn. The conditional likelihood for one image is formulated as follows:

$$P(\mathbf{y}|\mathbf{x}) = \frac{1}{Z(\mathbf{x})} \exp[-E(\mathbf{y}, \mathbf{x})]. \quad (1)$$

Here Z is the partition function, defined as:

$$Z(\mathbf{x}) = \sum_{\mathbf{y}} \exp[-E(\mathbf{y}, \mathbf{x})]. \quad (2)$$

One Unary/Pairwise Potential Network:

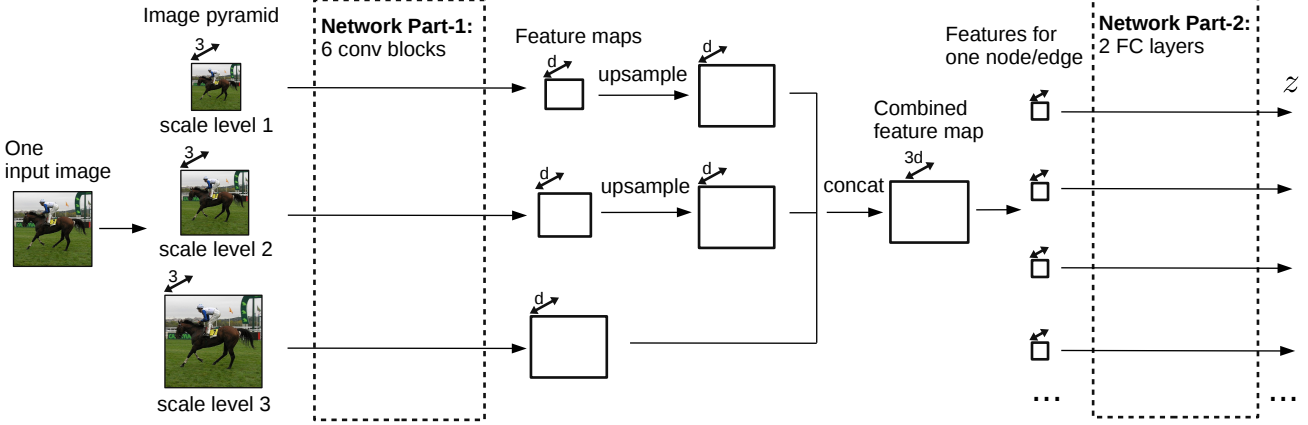


Fig. 4 – An illustration of the details of one unary or one pairwise potential network. An input image is first resized into 3 scales, then each resized image goes through 6 convolution blocks to output 3 feature maps. Then a CRF graph is constructed and node or edge features are generated from the feature maps. Node or edge features go through a network to generate the unary or pairwise potential network outputs. Finally the network outputs are fed into a CRF loss function in the training stage, or an MAP inference objective for prediction.

Network Part-1:

Conv block 1:	Conv block 2:	Conv block 3:	Conv block 4:	Conv block 5:	Conv block 6:
3 x 3 conv 64	3 x 3 conv 128	3 x 3 conv 256	3 x 3 conv 512	3 x 3 conv 512	7 x 7 conv 4096
3 x 3 conv 64	3 x 3 conv 128	3 x 3 conv 256	3 x 3 conv 512	3 x 3 conv 512	3 x 3 conv 512
2 x 2 pooling	2 x 2 pooling	3 x 3 conv 256	3 x 3 conv 512	3 x 3 conv 512	3 x 3 conv 512
		2 x 2 pooling	2 x 2 pooling	2 x 2 pooling	

Network Part-2:

2 fully-connected layers:
Fc 512
Fc 21(unary) or Fc 441(pairwise)

Fig. 5 – The detailed configuration of networks. “Network Part-1” and “Network Part-2” are described in Fig. 4. Here “Network Part-2” contains two layers, with number of output units equal to the number of classes K (unary) or equal to K^2 (pairwise).

The energy function is typically formulated by a set of unary and pairwise potentials:

$$E(\mathbf{y}, \mathbf{x}) = \sum_{U \in \mathcal{U}} \sum_{p \in \mathcal{N}_U} U(y_p, \mathbf{x}_p) + \sum_{V \in \mathcal{V}} \sum_{(p,q) \in \mathcal{S}_V} V(y_p, y_q, \mathbf{x}_{pq}).$$

Here U is a unary potential function, and to make the exposition more general, we consider multiple types of unary potentials with \mathcal{U} the set of all such unary potentials. \mathcal{N}_U is a set of nodes for the potential U . Likewise, V is a pairwise potential function with \mathcal{V} the set of all types of pairwise potential. \mathcal{S}_V is the set of edges for the potential V . We aim to learn all potentials in a unified CNN framework.

a) *Unary potential functions:* We formulate the unary potential function as follows:

$$U(y_p, \mathbf{x}_p; \theta_U) = \sum_{k=1}^K \delta(k = y_p) z_{p,k}(\mathbf{x}; \theta_U). \quad (3)$$

Here $\delta(\cdot)$ is the indicator function, which equals 1 if the input is true and 0 otherwise; K is the number of classes; $z_{p,k}$ is the unary network output value that corresponds to the p -th node and the k -th class. As previously noted, the dimension of the unary network output for one node is K .

b) *Pairwise potential functions:* We formulate the pairwise potential function as follows:

$$V(y_p, y_q, \mathbf{x}_{pq}; \theta_V) = \sum_{k=1}^K \sum_{j=1}^K \delta(k = y_p) \delta(j = y_q) z_{p,q,k,j}(\mathbf{x}; \theta_V).$$

Here $z_{p,q,k,j}$ is the pairwise network output. It is the cost value for the node pair (p, q) when they are labeled with the class

value (k, j) , which measures the compatibility of the label pair (y_p, y_q) given the input image \mathbf{x} . θ_V is the corresponding set of CNN parameters for the potential V , which we need to learn. As previously noted, the dimension of the network output for one pairwise connection is K^2 .

Our formulation of pairwise potentials is thus very different from the Potts-model-based formulation in the existing methods of [2], [31]. The Potts-model-based pairwise potentials employ a special formulation for enforcing neighborhood smoothness. In contrast, our pairwise potentials model the semantic compatibility between two nodes with the output for every possible value of the label pair (y_p, y_q) individually parameterized by CNNs. Clearly, our formulation is in a general form without special restrictions.

c) *Asymmetric pairwise potentials:* As in [35], [16], modeling asymmetric relations requires learning asymmetric potential functions, of which the output should depend on the input order of a pair of nodes. In other words, the potential function is required to be capable for modeling different input orders. Typically (but not necessarily), we have the following case for asymmetric relations:

$$V(y_p, y_q, \mathbf{x}_{pq}) \neq V(y_q, y_p, \mathbf{x}_{qp}). \quad (4)$$

Ideally the potential V is learned from the training data. Here we discuss the asymmetric relation “above/below” as an example. We take advantage of the input pair order to indicate the spatial configuration of two nodes, thus the input $(y_p, y_q, \mathbf{x}_{pq})$ indicates the configuration that the node p is

spatially lies above the node q . Clearly, the potential function is required to model different input orders.

Conventional smoothness potentials are unable to model different input orders. In contrast, the asymmetric property is readily achieved with our general formulation of pairwise potentials. The edge features for the node pair (p, q) are generated from a concatenation of the corresponding features of nodes p and q (as in [19]), in that order. The potential output for every possible pairwise label combination for (p, q) is individually parameterized by the pairwise CNNs. These factors ensure that the edge response is order dependent, trivially satisfying the asymmetric requirement.

d) Prediction: To predict the labeling of a new image, we solve the maximum a posteriori (MAP) inference problem:

$$\mathbf{y}^* = \operatorname{argmax}_{\mathbf{y}} P(\mathbf{y}|\mathbf{x}). \quad (5)$$

Our CRF graph does not form a tree structure, nor are the potentials submodular, hence we need to apply an approximate inference algorithm. To address this we apply an efficient message passing algorithm which is based on the mean field approximation [20], [21]. The mean field algorithm constructs a simpler distribution $Q(\mathbf{y})$, e.g., a product of independent marginals: $Q(\mathbf{y}) = \prod Q_p(y_p)$, which minimizes the KL-divergence between the distribution $Q(\mathbf{y})$ and $P(\mathbf{y})$. In our experiment, we run 2 mean field iterations which takes 1.5 seconds per image. We observe that more iterations do not offer improvement.

A. CRF training

A common approach for CRF learning is to maximize the likelihood, or equivalently minimize the negative log-likelihood, written for one image as:

$$-\log P(\mathbf{y}|\mathbf{x}; \boldsymbol{\theta}) = E(\mathbf{y}, \mathbf{x}; \boldsymbol{\theta}) + \log Z(\mathbf{x}; \boldsymbol{\theta}). \quad (6)$$

Adding regularization to the CNN parameter $\boldsymbol{\theta}$, the optimization problem for CRF learning is:

$$\min_{\boldsymbol{\theta}} \frac{\lambda}{2} \|\boldsymbol{\theta}\|_2^2 - \sum_{i=1}^N \log P(\mathbf{y}^{(i)}|\mathbf{x}^{(i)}; \boldsymbol{\theta}). \quad (7)$$

Here $\mathbf{x}^{(i)}$, $\mathbf{y}^{(i)}$ denote the i -th training image and its segmentation mask; N is the number of training images; λ is the weight decay parameter. Substituting (6) into (7) yields:

$$\min_{\boldsymbol{\theta}} \frac{\lambda}{2} \|\boldsymbol{\theta}\|_2^2 + \sum_{i=1}^N \left[E(\mathbf{y}^{(i)}, \mathbf{x}^{(i)}; \boldsymbol{\theta}) + \log Z(\mathbf{x}^{(i)}; \boldsymbol{\theta}) \right]. \quad (8)$$

We can apply gradient-based methods to optimize the above problem for learning $\boldsymbol{\theta}$. The energy function $E(\mathbf{y}, \mathbf{x}; \boldsymbol{\theta})$ is constructed from CNNs, and its gradient $\nabla_{\boldsymbol{\theta}} E(\mathbf{y}, \mathbf{x}; \boldsymbol{\theta})$ easily computed by applying the chain rule as in conventional CNNs. However, the partition function Z brings difficulties for optimization. Its gradient is written:

$$\begin{aligned} \nabla_{\boldsymbol{\theta}} \log Z(\mathbf{x}; \boldsymbol{\theta}) &= \sum_{\mathbf{y}} \frac{\exp[-E(\mathbf{y}, \mathbf{x}; \boldsymbol{\theta})]}{\sum_{\mathbf{y}'} \exp[-E(\mathbf{y}', \mathbf{x}; \boldsymbol{\theta})]} \nabla_{\boldsymbol{\theta}} [-E(\mathbf{y}, \mathbf{x}; \boldsymbol{\theta})] \\ &= -\mathbb{E}_{\mathbf{y} \sim P(\mathbf{y}|\mathbf{x}; \boldsymbol{\theta})} \nabla_{\boldsymbol{\theta}} E(\mathbf{y}, \mathbf{x}; \boldsymbol{\theta}) \end{aligned} \quad (9)$$

Generally the size of the output space \mathcal{Y} is exponential in the number of nodes, which prohibits the direct calculation of Z and its gradient. If the graph is tree-structured, belief propagation can be applied for exact calculation; otherwise, approximation is required, and even this is generally computationally expensive.

Note that usually a large number of stochastic gradient descent (SGD) iterations are required for training CNNs. It would not be unusual for 1 million iterations to be performed, which would require inference over the network to be carried out 1 million times. If each such inference takes around 1 second (which, again, would not be unusual), the time spent on inference alone would be nearly 12 days. Reducing the time spent on inference would thus significantly improve the scalability, and practicality, of the algorithm.

B. Piecewise training of CRFs

Instead of directly solving the optimization in (8) for CRF learning, we instead apply an approximate CRF learning method. In the literature, there are two popular types of learning methods which approximate the CRF objective: pseudo-likelihood learning [1] and piecewise learning [33]. These methods do not involve marginal inference for gradient calculation, which significantly improves the efficiency of training. Decision tree fields [28] and regression tree fields [18] are based on pseudo-likelihood learning, while piecewise learning has been applied in the work [33], [19].

Here we develop this idea for the case of jointly training the CNNs and the CRF (we also address pseudo-likelihood learning in the supplementary material). In piecewise training, the original graph is decomposed into a number of disjoint small graphs in which each small graph only involves one potential function. The conditional likelihood for piecewise training is formulated as a number of independent likelihoods defined on individual potentials, written as:

$$P(\mathbf{y}|\mathbf{x}) = \prod_{U \in \mathcal{U}} \prod_{p \in \mathcal{N}_U} P_U(y_p|\mathbf{x}) \prod_{V \in \mathcal{V}} \prod_{(p,q) \in \mathcal{S}_V} P_V(y_p, y_q|\mathbf{x}).$$

The likelihood $P_U(y_p|\mathbf{x})$ is constructed from the unary potential U . Likewise, $P_V(y_p, y_q|\mathbf{x})$ is constructed from the pairwise potential V . P_U and P_V are written as:

$$P_U(y_p|\mathbf{x}) = \frac{\exp[-U(y_p, \mathbf{x}_p)]}{\sum_{y'_p} \exp[-U(y'_p, \mathbf{x}_p)]}, \quad (10)$$

$$P_V(y_p, y_q|\mathbf{x}) = \frac{\exp[-V(y_p, y_q, \mathbf{x}_{pq})]}{\sum_{y'_p, y'_q} \exp[-V(y'_p, y'_q, \mathbf{x}_{pq})]}. \quad (11)$$

The log-likelihood for piecewise training is then:

$$\begin{aligned} \log P(\mathbf{y}|\mathbf{x}) &= \sum_{U \in \mathcal{U}} \sum_{p \in \mathcal{N}_U} \log P_U(y_p|\mathbf{x}) \\ &\quad + \sum_{V \in \mathcal{V}} \sum_{(p,q) \in \mathcal{S}_V} \log P_V(y_p, y_q|\mathbf{x}). \end{aligned} \quad (12)$$

The optimization problem for piecewise training is to mini-

TABLE I – Segmentation results on the PASCAL VOC 2012 val set. We evaluate our method with different settings, and compare against several recent methods with available results on the validation set. Our full model performs the best.

method	training set	# train	IoU val set
ours-unary-1scale	VOC extra	10k	58.3
ours-unary-3scales	VOC extra	10k	65.5
ours-pairwise-1	VOC extra	10k	66.7
ours-pairwise-2	VOC extra	10k	66.4
ours-1unary+2pair	VOC extra	10k	67.8
ours-full	VOC extra	10k	70.3
Zoom-out [27]	VOC extra	10k	63.5
Deep-struct [31]	VOC extra	10k	64.1
DeepLab [2]	VOC extra	10k	59.8
DeepLab-CRF [2]	VOC extra	10k	63.7
DeepLab-M-CRF [2]	VOC extra	10k	65.2
DeepLab-M-C-L [2]	VOC extra	10k	68.7
BoxSup [4]	VOC extra	10k	63.8
BoxSup [4]	VOC extra + COCO	133k	68.1

minimize the negative log likelihood with regularization:

$$\min_{\theta} \frac{\lambda}{2} \|\theta\|_2^2 - \sum_{i=1}^N \left[\sum_{U \in \mathcal{U}} \sum_{p \in \mathcal{N}_U^{(i)}} \log P_U(y_p | \mathbf{x}^{(i)}; \theta_U) + \sum_{V \in \mathcal{V}} \sum_{(p,q) \in \mathcal{S}_V^{(i)}} \log P_V(y_p, y_q | \mathbf{x}^{(i)}; \theta_V) \right]. \quad (13)$$

Compared to the objective in (8) for direct maximum likelihood learning, the above objective does not involve the global partition function $Z(\mathbf{x}; \theta)$. To calculate the gradient of the above objective, we only need to individually calculate the gradient $\nabla_{\theta_U} \log P_U$ and $\nabla_{\theta_V} \log P_V$. With the definition in (10), P_U is a conventional Softmax normalization function over only K (the number of classes) elements. Similar analysis can also be applied to P_V . Hence, we can easily calculate the gradient without involving expensive inference. Moreover, we are able to perform paralleled training of potential functions, since the above objective is formulated by a summation of log-likelihoods which are defined on individual potentials.

Avoiding repeated inference is critical to tractable joint learning of CNNs and CRFs on large-scale data. As previously discussed, CNN training usually involves a large number of gradient update iteration which prohibit the repeated expensive inference. Moreover, context is generally a weaker cue than appearance, and thus large-scale training data is usually required for effective context learning. Our piecewise approach here provides a practical solution for CNN and CRF joint learning on large-scale data.

V. EXPERIMENTS

We evaluate our method on the PASCAL VOC 2012 dataset [10] which consists of 20 object categories and one background category. This dataset is split into a training set, a validation set and a test set, which respectively contain 1464, 1449 and 1456 images. Following a conventional setting in [15], [2], the training set is augmented by extra annotated VOC images provided in [14], which results in 10582 training images. The segmentation performance is measured by the intersection-over-union (IoU) score [10].

A. Implementation details

The first 5 convolution blocks and the first convolution layer in the 6th convolution block are initialized from the VGG-16 model [32]. This model is also applied in most of the comparison methods. All remaining layers are randomly initialized. All layers are trained using back-propagation. The learning rate for randomly initialized layers is set to 0.001; for VGG-16 initialized layers it is set to a smaller value: 0.0001. We use 3 scales for the input image: 1.2, 0.8 and 0.4, which is selected through cross validation.

As illustrated in Fig. 3, in practice we currently use 2 types of pairwise potential functions. The range box size is adapted to the size of the input image. We denote by a the length of the shortest edge of the largest feature map. For the potential “Pairwise-1”, the range box size is $0.4a \times 0.4a$, and it is centered on the node. For the potential: “Pairwise-2”, the range box size is $0.3a \times 0.4a$ and the bottom edge of the box is centered on the node.

B. Evaluation of different settings

We first evaluate our method with different parameter settings. Table I shows the results on the PASCAL VOC 2012 validation set compared to a number of recent methods which have reported results on the validation set.

The first two rows show the results of our unary-only models contrasting the use of 1 image scale and 3 image scales (denoted by “ours-unary-1scale” and “ours-unary-3scales” in the table). Clearly the 3-scale setting achieves markedly superior performance. This verifies our earlier claim that the multi-scale network architecture captures rich background contextual information, significantly improving the prediction performance. Unless otherwise specified, we report the use of 3 image scale features for all types of unary or pairwise potentials in subsequent results.

Table I also provides a comparison of the performance using only one type of potential function (either unary alone, or one pairwise potential, alone). It shows that our method using a single type of potential function already outperforms many other methods which use the same augmented PASCAL VOC dataset provided in [14]. In particular, the pairwise potential functions with context learning show better performance than the unary potential function. Combining all potential functions, our performance (denoted by “ours-1unary+2pair”) is further improved. Overall the results clearly support our claim that exploring different types of context (spatial context and object-background context) helps to improve the performance.

Finally, to refine our predictions further, we apply the post-processing technique proposed in [21], which has also been used in the comparing method DeepLab [2] and BoxSup [4]. This post-processing step incorporates the high-level semantic predictions and the low-level pixel values for smoothness based refinement, resulting in sharp prediction on object boundaries. In this table, DeepLab-CRF is the FCNN based method DeepLab with the dense CRF method in [21] for post-processing. Following FCN-8s [26], DeepLab-M-CRF improves DeepLab-CRF by incorporating multi-scale features.

TABLE II – Individual category results of our method on the PASCAL VOC 2012 validation set using different settings. Best performed potential functions are marked in gray color. The potential functions show different preferences on categories. The gained performance scores of the potential function pairwise-1 and pairwise-2 over the unary model are shown.

method	mean	aero	bike	bird	boat	bottle	bus	car	cat	chair	cow	table	dog	horse	mbike	person	potted	sheep	sofa	train	tv
unary-1scale	58.3	71.2	32.4	66.9	53.5	55.8	72.9	70.8	73.1	25.3	54.6	38.5	64.1	55.3	66.9	73.4	40.6	61.3	30.2	69.5	58.1
unary-3scales	65.5	76.3	35.7	74.3	58.8	70.4	85.3	81.3	79.1	30.1	62.3	43.5	69.9	67.3	73.7	77.9	49.9	71.8	36.6	76.7	62.9
pairwise-1	66.7	80.0	34.5	78.1	58.4	67.9	88.5	82.0	81.0	32.1	62.9	50.5	76.2	67.8	71.9	77.9	50.0	70.1	35.3	77.8	65.6
gain over unary		3.7		3.8			3.2	0.7	1.9	2.0	0.6	7.0	6.3	0.5			0.1			1.1	2.7
pairwise-2	66.4	78.3	33.0	76.3	59.6	70.4	86.8	81.5	79.7	30.3	61.8	48.0	76.1	62.6	75.3	78.0	53.0	66.8	38.6	79.1	68.1
gain over unary		2.0		2.0	0.8		1.5	0.2	0.6	0.2	4.5	6.2			1.6	0.1	3.1		2.0	2.4	5.2
1unary+2pair	67.8	80.7	35.6	77.9	59.6	71.4	88.5	83.1	81.1	32.1	64.0	50.6	76.3	67.5	75.1	79.5	52.0	72.2	37.4	79.6	66.7
full	70.3	86.7	36.9	82.3	63.0	74.2	89.8	84.1	84.1	32.8	65.4	52.1	79.7	72.1	77.6	81.7	55.6	77.4	37.4	81.4	68.4

DeepLab-M-C-F [2] is an improved version of DeepLab-M-CRF, whose result is recently reported by the authors. Our final performance (denoted by “ours-full”) achieves 70.3 IoU score on the validation set (Table I), which is significantly better than all other compared methods. The recent method BoxSup [4] explores the COCO dataset together with the VOC augmented dataset. The COCO dataset [23] consists of 133K images which is much larger than the VOC dataset. The result shows that our method still outperforms BoxSup, although we use much less training data.

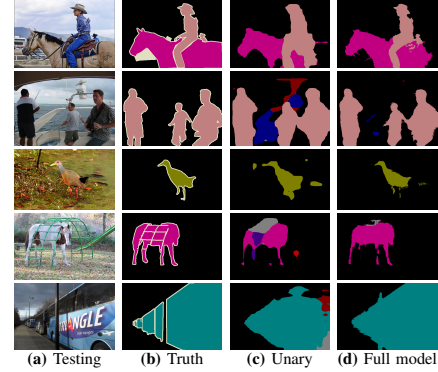


Fig. 6 – Comparison between the unary-only model and our full model. Our full model shows better performance.

C. Detailed evaluation of potentials

We perform category-level evaluation and compare different types of potential functions in this section. The results for each category are shown in Table II. We first evaluate our method with different settings. We compare our unary-only models with one image scale and 3 image scales. It clearly shows that all categories benefit from using 3 image scales which take advantage of rich background context.

We further evaluate different types of potential functions in Table II. The potential “pairwise-1” captures the “surrounding” spatial relations; the potential “pairwise-2” captures the “above/below” spatial relations; “1unary+2pair” is the combined model; “full” indicates our final model. The gained scores of “pairwise-1” and “pairwise-2” over the unary model are reported in the table.

We compare the performance of only using one type of potential function. Best performed potential functions are marked in gray color. The potential functions show different performance on categories. The potential “pairwise-1” performs the best in 10 out of 20 categories, while “pairwise-2” performs the best in the other 7 categories. It shows that the potential functions are able to capture different kinds of contextual information. Hence combining them results in better overall performance. The categories: dining table, dog, TV/monitor, aeroplane, bird, bus, and potted plant gain significantly benefits from the pairwise model (pairwise-1 or pairwise-2) which explores spatial relations.

We compare some segmentation examples of the unary-only model and the full model in Fig. 6. It shows that our full model with context learning significantly improves the performance. More prediction examples of our final model are shown in Fig. 7 and the supplementary document.

TABLE III – Segmentation results on the PASCAL VOC 2012 test set. Compared to methods that use the same augmented VOC dataset, our method has the second best performance. Compared to methods trained on extra COCO dataset, our method achieves comparable performance, while using much less training data.

method	training set	# train	IoU test set
Zoom-out [27]	VOC extra	10k	64.4
FCN-8s [26]	VOC extra	10k	62.2
SDS [15]	VOC extra	10k	51.6
CRF-RNN [36]	VOC extra	10k	65.2
DeepLab-CRF [2]	VOC extra	10k	66.4
DeepLab-M-CRF [2]	VOC extra	10k	67.1
DeepLab-M-C-L [2]	VOC extra	10k	71.6
DeepLab-CRF [29]	VOC extra + COCO	133k	70.4
DeepLab-M-C-L [29]	VOC extra + COCO	133k	72.7
BoxSup (semi) [4]	VOC extra + COCO	133k	71.0
ours	VOC extra	10k	70.7

D. Comparison on the test set

We further verify our performance on the PASCAL VOC 2012 test set. We compare with a number of recent methods which have competitive performance. The results are described in Table III. Since the ground truth labels are not available for the test set, we evaluate our method through the VOC evaluation server. We achieve a very impressive result on the test set: 70.7 IoU score¹. Compared to the methods that use the same augmented PASCAL VOC dataset provided in [14], we outperform all methods except DeepLab-M-C-L [2]. The result of DeepLab-M-C-L is very recently reported by the authors, which is concurrent to our work here. We also include

¹ The result link provided by the VOC evaluation server: <http://host.robots.ox.ac.uk:8080/anonymous/XCG9OR.html>

TABLE IV – Individual category results on the PASCAL VOC 2012 test set. Our method achieves on par performance with DeepLab-M-C-L (wins 10 out of 20 categories), and outperforms FCN-8s and DeepLab-CRF.

method	mean	aero	bike	bird	boat	bottle	bus	car	cat	chair	cow	table	dog	horse	mbike	person	potted	sheep	sofa	train	tv
DeepLab-CRF [2]	66.4	78.4	33.1	78.2	55.6	65.3	81.3	75.5	78.6	25.3	69.2	52.7	75.2	69.0	79.1	77.6	54.7	78.3	45.1	73.3	56.2
DeepLab-M-C-L [2]	71.6	84.4	54.5	81.5	63.6	65.9	85.1	79.1	83.4	30.7	74.1	59.8	79.0	76.1	83.2	80.8	59.7	82.2	50.4	73.1	63.7
FCN-8s [26]	62.2	76.8	34.2	68.9	49.4	60.3	75.3	74.7	77.6	21.4	62.5	46.8	71.8	63.9	76.5	73.9	45.2	72.4	37.4	70.9	55.1
ours	70.7	87.5	37.7	75.8	57.4	72.3	88.4	82.6	80.0	33.4	71.5	55.0	79.3	78.4	81.3	82.7	56.1	79.8	48.6	77.1	66.3

the comparison with methods that trained on the much larger COCO dataset (133K training images). Our performance is comparable with these methods, while our method uses much less training images.

The results for each category is shown in Table IV. We compare with several most relevant methods: DeepLab-CRF [2], DeepLab-M-C-L [2] and FCN-8s [26], which are all fully-CNN based methods and transfer layers from the same VGG-16 model. It clearly shows that our method outperforms FCN-8s and DeepLab by a large margin. We outperform DeepLab-M-C-L in 10 out of 20 categories, thus we have on par performance with DeepLab-M-C-L.

E. Discussion

We have evaluated our deep CRF models from various aspects. We summary the key points for good performance:

- Learning multi-scale FCNNs from multi-scale image inputs to capture rich background context.
- Learning multiple contextual pairwise potentials. Different types of pairwise potentials are able to exploit different aspects of the spatial context.

Learning spatial context is also addressed in the method TAS [17]. TAS and our method are both concerned with modeling different types of spatial context, e.g., stuff-object context, and consider various spatial relations, although these two methods apply completely different techniques. TAS explicitly models different classes of the background regions with unsupervised clustering. In contrast, our approach learns the stuff-object context without explicitly formulating different types of background regions. This information might be implicitly captured in our networks. Extending our method with explicitly background classes modeling can be a future direction. This extension might have benefits on intuitive explanation on what the contextual model has learned. For example, we are probably able to discover a “road” class with unsupervised learning, which support the prediction of cars in neighboring regions.

VI. CONCLUSIONS

We have proposed a method which jointly learns FCNNs and CRFs to exploit *complex* contextual information for semantic image segmentation. We formulate FCNN based pairwise potentials for modeling complex spatial relations between image regions, and use multi-scale networks to exploit background context. Our method shows competitive performance on the PASCAL VOC 2012 dataset.

One future direction will be to consider the possibility of extracting *explicit* information about the different background

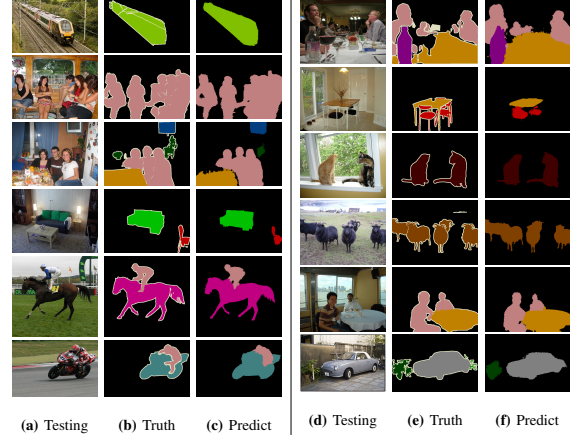


Fig. 7 – Some prediction examples of our method.

contexts that are captured by the networks. More generally our formulation is potentially widely applicable, so we naturally aim to apply the proposed deep CRFs with piecewise training to other vision tasks.

APPENDIX

CRF pseudo-likelihood training [1] is an alternative to piecewise training for efficient CRF learning, which has been applied in decision tree fields [28] and regression tree fields [18]. Pseudo-likelihood training approximates the original likelihood by the product of the likelihood functions defined on individual nodes. The likelihood function for one node is conditioned on all remaining nodes. The likelihood function for each node can be independently optimized. The conditional likelihood for pseudo-likelihood training is written as:

$$P(\mathbf{y}|\mathbf{x}) = \prod_{p \in \mathcal{N}} P(y_p | \bar{\mathbf{y}}_p, \mathbf{x}). \quad (14)$$

Here $\bar{\mathbf{y}}_p$ is the output variables exclude the y_p . The log-likelihood is written as:

$$\begin{aligned} \log P(\mathbf{y}|\mathbf{x}; \boldsymbol{\theta}) &= \log \prod_{p \in \mathcal{N}} P(y_p | \bar{\mathbf{y}}_p, \mathbf{x}; \boldsymbol{\theta}) \\ &= \log \prod_{p \in \mathcal{N}} \frac{1}{Z_p(\mathbf{x}; \boldsymbol{\theta})} \exp[-E(\mathbf{y}, \mathbf{x}; \boldsymbol{\theta})] \\ &= \sum_{p \in \mathcal{N}} -E(y_p, \bar{\mathbf{y}}_p, \mathbf{x}; \boldsymbol{\theta}) - \log Z_p(\mathbf{x}; \boldsymbol{\theta}). \end{aligned} \quad (15)$$

Here Z_p is the partition function in the likelihood function for the node p , which is written as:

$$Z_p(\mathbf{x}; \boldsymbol{\theta}) = \sum_{y_p} \exp[-E(y_p, \bar{\mathbf{y}}_p, \mathbf{x}; \boldsymbol{\theta})]. \quad (16)$$

The optimization problem for pseudo-likelihood training is to minimize the negative log-likelihood with regularization, which is written as:

$$\min_{\boldsymbol{\theta}} \frac{\lambda}{2} \|\boldsymbol{\theta}\|_2^2 + \sum_{i=1}^N \sum_{p \in \mathcal{N}^{(i)}} \left[E(y_p^{(i)}, \bar{\mathbf{y}}_p^{(i)}, \mathbf{x}^{(i)}; \boldsymbol{\theta}) + \log Z_p(\mathbf{x}^{(i)}; \boldsymbol{\theta}) \right]. \quad (17)$$

For CNNs and CRFs joint training, we need to calculate the gradient of the above objective. The gradient of $E(\cdot)$ can be efficiently calculated by network back-propagation. Note that Z_p only involves one output variable, hence it is efficient to calculate Z_p and its gradient. The gradient of $\log Z_p(\mathbf{x}; \boldsymbol{\theta})$ is:

$$\begin{aligned} \nabla_{\boldsymbol{\theta}} \log Z_p(\mathbf{x}; \boldsymbol{\theta}) &= \nabla_{\boldsymbol{\theta}} \log \sum_{y_p} \exp[-E(y_p, \bar{\mathbf{y}}_p, \mathbf{x})] \\ &= - \sum_{y_p} \frac{\exp[-E(y_p, \bar{\mathbf{y}}_p, \mathbf{x}; \boldsymbol{\theta})]}{\sum_{y'_p} \exp[-E(y'_p, \bar{\mathbf{y}}_p, \mathbf{x}; \boldsymbol{\theta})]} \nabla_{\boldsymbol{\theta}} E(y_p, \mathbf{x}; \boldsymbol{\theta}) \\ &= - \sum_{y_p} P(y_p | \bar{\mathbf{y}}_p, \mathbf{x}; \boldsymbol{\theta}) \nabla_{\boldsymbol{\theta}} E(y_p, \mathbf{x}; \boldsymbol{\theta}). \end{aligned} \quad (18)$$

We observe that piecewise training is able to achieve better performance and faster convergence than pseudo-likelihood training. Thus we apply piecewise training throughout our experiments.

The CRF graph is constructed based on the size of the largest feature map which is generated by the last convolution block. One node in the graph corresponds to one spatial position in this feature map. For each node we use a rectangle box to specify the neighborhood range for pairwise connections.

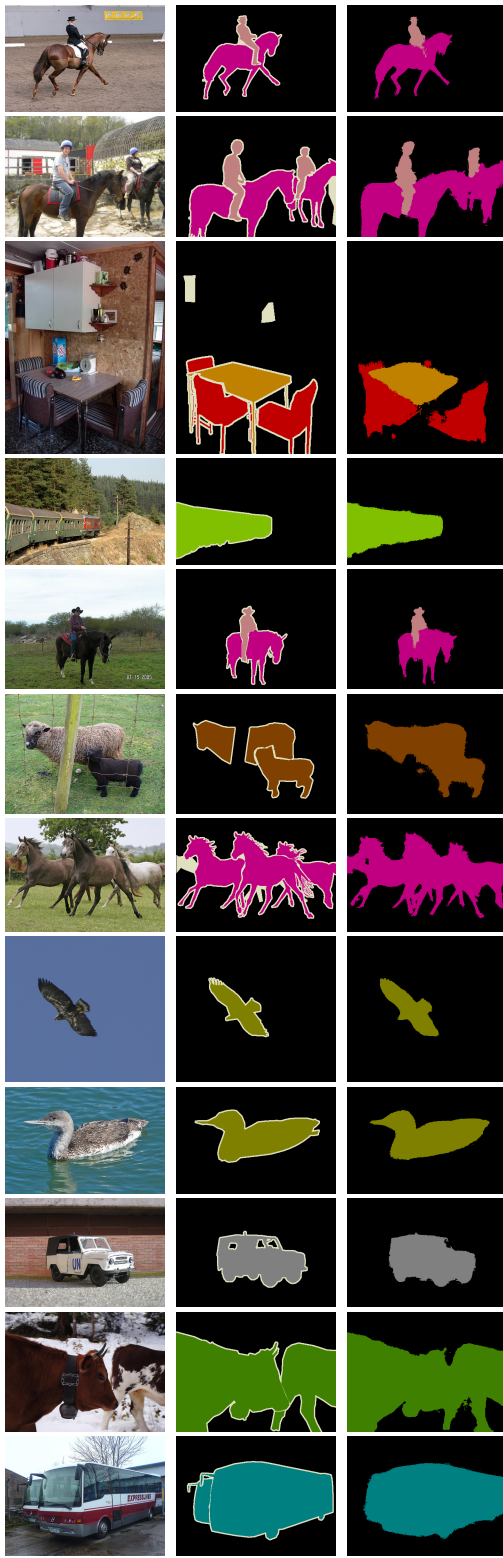
The weight decay parameter is set to 0.0005; the momentum parameter is set to 0.9. The learning rate for one epoch is decreased by multiplying 0.97 to the learning rate of the previous epoch.

Due to the operators of convolution and pooling strides, the final convolution feature map is smaller than the size of the input image, thus we perform down-sampling of the ground-truth for training and up-sampling the labeling mask for prediction. In the training stage, the ground truth mask is resized to match the largest feature map by nearest neighbor down-sampling; in the prediction stage, the prediction confidence score map is up-sampled by bilinear interpolation to match the size of the input image.

More segmentation examples of our final model are demonstrated in Fig. 8, and Fig. 9. A few failed examples are shown in Fig. 10. Some failed predictions are caused by the limitation of the ground truth. For example, a laptop screen is not considered as an object in the ground truth, but we predict it as TV/monitor.



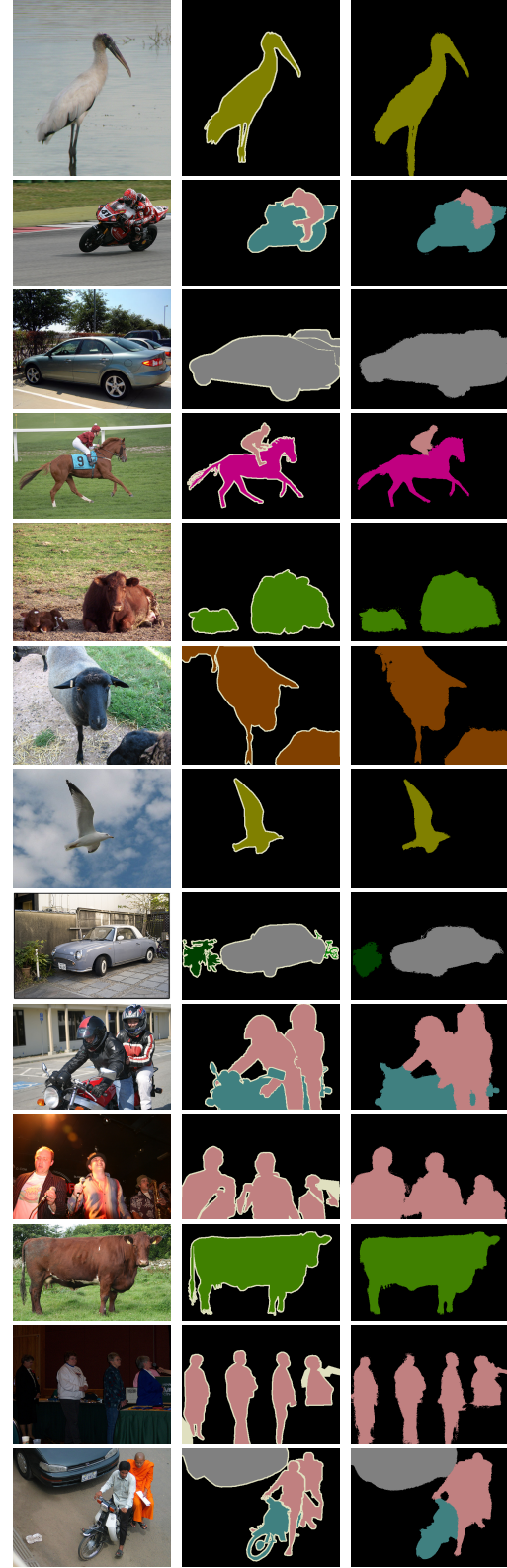
Fig. 8 – Some prediction examples of our method.



(a) Testing

(b) Truth

(c) Prediction



(d) Testing

(e) Truth

(f) Prediction

Fig. 9 – Some prediction examples of our method.

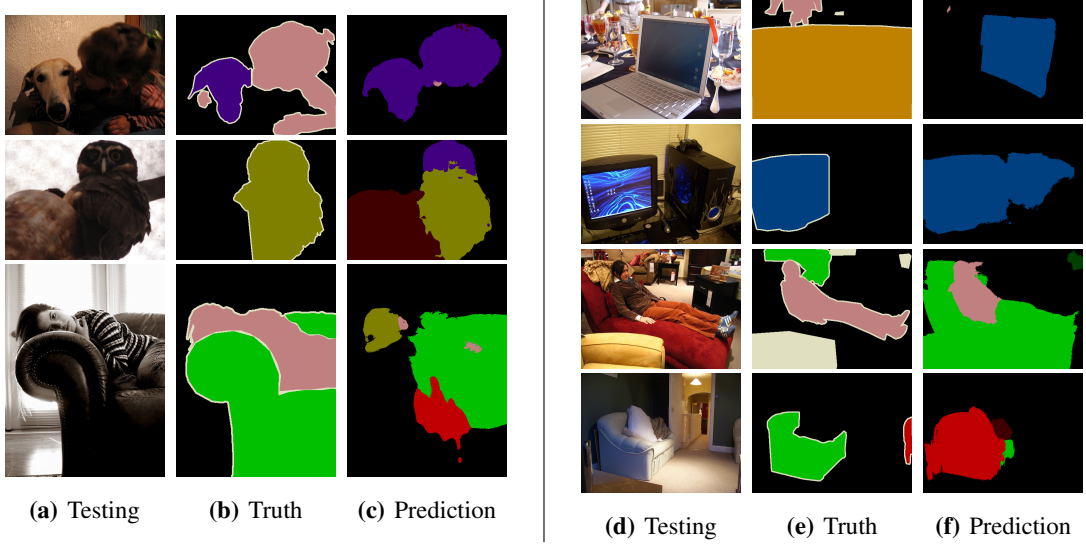


Fig. 10 – Some prediction examples of our method with weak performance.

REFERENCES

- [1] J. Besag, "Efficiency of pseudolikelihood estimation for simple Gaussian fields," *Biometrika*, 1977.
- [2] L. Chen, G. Papandreou, I. Kokkinos, K. Murphy, and A. L. Yuille, "Semantic image segmentation with deep convolutional nets and fully connected CRFs," 2014. [Online]. Available: <http://arxiv.org/abs/1412.7062>
- [3] L.-C. Chen, A. G. Schwing, A. L. Yuille, and R. Urtasun, "Learning deep structured models," 2014. [Online]. Available: <http://arxiv.org/abs/1407.2538>
- [4] J. Dai, K. He, and J. Sun, "BoxSup: Exploiting bounding boxes to supervise convolutional networks for semantic segmentation," 2015. [Online]. Available: <http://arxiv.org/abs/1503.01640>
- [5] S. K. Divvala, D. Hoiem, J. H. Hays, A. A. Efros, and M. Hebert, "An empirical study of context in object detection," in *IEEE Conference on Computer Vision and Pattern Recognition*, 2009.
- [6] C. Doersch, A. Gupta, and A. A. Efros, "Context as supervisory signal: Discovering objects with predictable context," in *Proc. European Conf. Computer Vision*, 2014.
- [7] C. Dong, C. C. Loy, K. He, and X. Tang, "Learning a deep convolutional network for image super-resolution," in *Proc. Eur. Conf. Comp. Vis.*, 2014.
- [8] D. Eigen, D. Krishnan, and R. Fergus, "Restoring an image taken through a window covered with dirt or rain," in *Proc. Int. Conf. Comp. Vis.*, 2013.
- [9] D. Eigen, C. Puhrsch, and R. Fergus, "Depth map prediction from a single image using a multi-scale deep network," in *Proc. Adv. Neural Info. Process. Syst.*, 2014.
- [10] M. Everingham, L. Van Gool, C. K. Williams, J. Winn, and A. Zisserman, "The pascal visual object classes (voc) challenge," *Int. J. Comp. Vis.*, 2010.
- [11] C. Farabet, C. Couprie, L. Najman, and Y. LeCun, "Learning hierarchical features for scene labeling," *IEEE T. Pattern Analysis Mach. Intelli.*, 2013.
- [12] D. A. Forsyth, J. Malik, M. M. Fleck, H. Greenspan, T. K. Leung, S. Belongie, C. Carson, and C. Bregler, "Finding pictures of objects in large collections of images," in *ECCV Workshop on Object Representation in Computer Vision II*, 1996.
- [13] R. B. Girshick, J. Donahue, T. Darrell, and J. Malik, "Rich feature hierarchies for accurate object detection and semantic segmentation," in *Proc. IEEE Conf. Comp. Vis. Pattern Recogn.*, 2014.
- [14] B. Hariharan, P. Arbelaez, L. D. Bourdev, S. Maji, and J. Malik, "Semantic contours from inverse detectors," in *Proc. Int. Conf. Comp. Vis.*, 2011.
- [15] B. Hariharan, P. Arbeláez, R. Girshick, and J. Malik, "Simultaneous detection and segmentation," in *Proc. European Conf. Computer Vision*, 2014.
- [16] D. Heesch and M. Petrou, "Markov random fields with asymmetric interactions for modelling spatial context in structured scene labelling," *Journal of Signal Processing Systems*, 2010.
- [17] G. Heitz and D. Koller, "Learning spatial context: Using stuff to find things," in *Proc. European Conf. Computer Vision*, 2008.
- [18] J. Jancsary, S. Nowozin, T. Sharp, and C. Rother, "Regression tree fields: an efficient, non-parametric approach to image labeling problems," in *Proc. IEEE Conf. Comp. Vis. Pattern Recogn.*, 2012.
- [19] A. Kolesnikov, M. Guillaumin, V. Ferrari, and C. H. Lampert, "Closed-form training of conditional random fields for large scale image segmentation," in *Proc. Eur. Conf. Comp. Vis.*, 2014.
- [20] D. Koller and N. Friedman, *Probabilistic graphical models: principles and techniques*. MIT Press, 2009.
- [21] P. Krähenbühl and V. Koltun, "Efficient inference in fully connected CRFs with Gaussian edge potentials," in *Proc. Adv. Neural Info. Process. Syst.*, 2012.
- [22] —, "Parameter learning and convergent inference for dense random fields," in *Proc. Int. Conf. Mach. Learn.*, 2013.
- [23] T.-Y. Lin, M. Maire, S. Belongie, J. Hays, P. Perona, D. Ramanan, P. Dollár, and C. L. Zitnick, "Microsoft COCO: Common objects in context," in *Proc. Eur. Conf. Comp. Vis.*, 2014.
- [24] F. Liu, C. Shen, and G. Lin, "Deep convolutional neural fields for depth estimation from a single image," in *Proc. IEEE Conf. Comp. Vis. Pattern Recogn.*, 2015.
- [25] F. Liu, C. Shen, G. Lin, and I. Reid, "Learning depth from single monocular images using deep convolutional neural fields," 2015. [Online]. Available: <http://arxiv.org/abs/1502.07411>
- [26] J. Long, E. Shelhamer, and T. Darrell, "Fully convolutional networks for semantic segmentation," in *Proc. IEEE Conf. Comp. Vis. Pattern Recogn.*, 2015.
- [27] M. Mostajabi, P. Yadollahpour, and G. Shakhnarovich, "Feedforward semantic segmentation with zoom-out features," 2014. [Online]. Available: <http://arxiv.org/abs/1412.0774>
- [28] S. Nowozin, C. Rother, S. Bagon, T. Sharp, B. Yao, and P. Kohli, "Decision tree fields," in *Proc. Int. Conf. Comp. Vis.*, 2011.
- [29] G. Papandreou, L.-C. Chen, K. Murphy, and A. L. Yuille, "Weakly- and semi-supervised learning of a DCNN for semantic image segmentation," 2015. [Online]. Available: <http://arxiv.org/abs/1502.02734>
- [30] A. Rabinovich, A. Vedaldi, C. Galleguillos, E. Wiewiora, and S. Belongie, "Objects in context," in *Proc. Int. Conf. Comp. Vis.*, 2007.
- [31] A. G. Schwing and R. Urtasun, "Fully connected deep structured networks," 2015. [Online]. Available: <http://arxiv.org/abs/1503.02351>
- [32] K. Simonyan and A. Zisserman, "Very deep convolutional networks for large-scale image recognition," 2014. [Online]. Available: <http://arxiv.org/abs/1409.1556>
- [33] C. A. Sutton and A. McCallum, "Pieewise training for undirected models," in *Proc. Conf. Uncertainty Artificial Intelli.*, 2005.
- [34] J. Tompson, A. Jain, Y. LeCun, and C. Bregler, "Joint training of a convolutional network and a graphical model for human pose estimation," in *Proc. Adv. Neural Info. Process. Syst.*, 2014.
- [35] J. Winn and J. Shotton, "The layout consistent random field for recognizing and segmenting partially occluded objects," in *Proc. IEEE Conf. Comp. Vis. Pattern Recogn.*, 2006.
- [36] S. Zheng, S. Jayasumana, B. Romera-Paredes, V. Vineet, Z. Su, D. Du, C. Huang, and P. Torr, "Conditional random fields as recurrent neural networks," 2015. [Online]. Available: <http://arxiv.org/abs/1502.03240>